Geometrical optimisation of vehicle shock dampers with magnetorheological fluid

Zekeriya Parlak*, Tahsin Engin and Vedat Arı

Department of Mechanical Engineering,
Sakarya University,
54187 Esentepe Campus, Sakarya, Turkey
E-mail: zparlak@sakarya.edu.tr
E-mail: engint@sakarya.edu.tr
E-mail: vedatari@sakarya.edu.tr
*Corresponding author

İsmail Şahin

Vocational School of Akyazi,
Sakarya University,
Alagac Cad. Akyazi, Sakarya, Turkey
E-mail: isahin@sakarya.edu.tr

İsmail Çallı

Department of Mechanical Engineering,
Sakarya University,
54187 Esentepe Campus, Sakarya, Turkey
E-mail: calli@sakarya.edu.tr

Abstract: Magnetorheological (MR) dampers have attracted interest from suspension designers and researchers because of their variable damping feature, mechanical simplicity, robustness, low power consumption and fast response. Therefore, optimisation of such devices is of particular interest to achieve optimal vibration control. This study deals with the geometrical optimisation of an MR shock damper using Taguchi experimental design approach. The optimal solutions of the MR damper were evaluated using analytical equations, which give the dynamic range of the damper under consideration. Optimal geometrical values obtained provided most performance in consideration of other nine alternatives of Taguchi experimental design specified for the study.

Keywords: magnetorheological shock damper; MR damper; MR devices; MR fluid; optimisation; Taguchi method; design.

Reference to this paper should be made as follows: Parlak, Z., Engin, T., Arı, V., Şahin, İ. and Çallı, İ. (2010) 'Geometrical optimisation of vehicle shock dampers with magnetorheological fluid', *Int. J. Vehicle Design*, Vol. 54, No. 4, pp.371–392.

Biographical notes: Zekeriya Parlak was awarded his BS and MS in Mechanical Engineering from Trakya University and Sakarya University (Turkey) in 1998 and 2004, respectively. He is now a PhD student at Sakarya University. His PhD research project has involved developing dynamic models and geometrical optimisation of a magnetorheological damper.

Tahsin Engin obtained his BS and MS in Mechanical Engineering from Hacetepe University and Karaelmas University (Turkey) in 1992 and 1995, respectively, and his Doctorate in Mechanical Engineering from Sakarya University (Turkey) in 2000. He is now Associate Professor of Mechanical Engineering at Sakarya University, with research interests on tip clearance effects in centrifugal pumps and fans, solid–liquid flow through the pumps, hydraulic transportation of solids, thermal engineering optimisation, thermal and fluid flow considerations in process engineering, Newtonian and non-Newtonian fluid flows in microchannels and magnetorheological fluid flow considerations.

Vedat Arı obtained his BS in Mechanical Education from Technical Education Faculty of Gazi University and MS in Mechanical Education from Dumlupınar University, and his Doctorate in Mechanical Education from Sakarya University (Turkey) in 2000. He is now Assistant Professor of Mechanical Education in Technical Education Faculty at Sakarya University, with research interests on tip clearance effects in centrifugal pumps and fans, solid–liquid flow through the pumps, hydraulic transportation of solids, thermal engineering optimisation, thermal and fluid flow considerations in process engineering, energy and exergy approachment of cement process and cyclone design systems.

İsmail Şahin is an Assistant Professor of Vocational School of Akyazi at Sakarya University. He obtained his BS in Machine Teaching from Gazi University, his MS in Machine Teaching from Dumlupinar University and PhD in Machine Teaching from Sakarya University in 1993, 1996 and 2005, respectively. His research interests focus on magnetorheological dampers and applications, semi-active suspension systems, computer-aided designs and analysis and machine construction.

İsmail Çallı is a Professor of Mechanical Engineering at Sakarya University. He received his BS and MS in Mechanical Engineering from Istanbul Technical University, Turkey, in 1971 and 1973, respectively, and his Doctorate in Mechanical Engineering from Yildiz Technical University (Turkey) in 1986. His research interests focus on hydraulic and pneumatic systems.

1 Introduction

Magnetorheological (MR) fluids are suspensions of magnetically polarisable particles with a few microns in size dispersed in a carrying liquid such as mineral or silicon oil. When a magnetic field is applied to the fluid, particles in the fluid form chains, and the suspension becomes like a semi-solid material owing to increase in the yield stress. Under the magnetic field, an MR fluid behaves as a non-Newtonian fluid with controllable viscosity. However, if the magnetic field is removed, the suspension turns to a Newtonian fluid in a few milliseconds, and the transition between these two phases is highly reversible, which provides unique feature of magnetic-field controllability of the flow of MR fluids.

MR devices have been used for vibration suppression, automation, shock isolation and machining methods in a wide range of industries. Although there are a large number of papers on the design and characterisation of both MR and ER dampers, no systematic study on the optimisation of such important devices is available in the open literature. This is presumably due to the fact that a lot of design parameters need to be considered in developing of MR dampers to obtain optimal geometry, which makes the problem very challenging when using conventional optimisation methods. Controllability of MR devices is provided with applied different magnetic fields across a gap through which MR fluid flows. When MR fluid within the gap is activated, the development of the yield stress binds a volume of fluid into a solid plug. The remaining unbound fluid then experiences greater shear forces, which in turn results in a greater pressure drop across the device (Rosenfeld and Wereley, 2004).

Typically, MR devices have generally one annular gap through which fluid is forced, but this is not a strict constraint. In numerous papers, single rectangular (Wereley and Pang, 1998; Spencer et al., 1998; Jolly et al., 1999) and annular ducts (Rosenfeld and Wereley, 2004; Nguyen and Choi, 2009a; Yang et al., 2008; Nguyen et al., 2007, 2008) were employed in the devices. Similarly, Stanway et al. (1996) and Namuduri et al. (2001) proposed concentric multiple annular flow gaps.

The fail-safe design feature is accomplished by selecting appropriate channel flow geometry to obtain the minimum required viscous (passive) damping force at zero magnetic field (Hitchcock, 2002). It was assumed in that paper that the off-state damping requirement had been fixed (e.g., by safety requirements for minimum damping), and that the damper should achieve the greatest possible on-state damping (Rosenfeld and Wereley, 2004).

Magnetic design, on the other hand, is of particular interest to achieve optimal performance of the MR damper. Hitchcock (2002) performed a 3D FEM analysis, and reported that the magnetic field direction should be perpendicular to MR fluid flow direction. Zhang et al. (2006) proposed a design method for the MR dampers based on FEM. They showed that through experimental verification, the damper force was effectively scaled by the magnetic design.

Rosenfeld and Wereley (2004) proposed an optimisation method on a volume-constrained MR valve. Their method was an analytical optimisation design method for MR valves and dampers relying upon the assumption of constant magnetic flux density throughout the magnetic circuit. Nguyen et al. (2007) applied the optimal design model for single-coil, two-coil, three-coil and radial–annular types of MR valves constrained in a specified volume. They found that two-coil MR valve provided the best value of valve ratio while the annular–radial type provides the best pressure drop at the optimal design parameters. Nguyen et al. (2008) proposed a similar model for MR valve but considering control energy as well as time response.

Yang et al. (2008) introduced an MR smart structure design method. In their optimisation procedure, objective function was selected as the damping force, and volume fraction, target time constant, magnetic field intensity, wire winding turns and lost power were chosen as constraints. They determined the optimal values for damping force, magnetic field intensity, time constant and lost power for various wire winding turns at constant cylinder diameter, length and gap.

Nguyen and Choi (2009b) presented an optimal design of an MR shock absorber based on FEM. The MR shock absorber was constrained in a specific volume and the optimisation problem identified the geometric dimensions of the shock absorber that minimise a multi-objective function. They determined the optimal values for coil width, flange thickness, piston radius and gap width.

This study deals with the optimal sizing of the MR dampers using Taguchi Design of Experiments (DOE) method. For this purpose, an MR damper has been modelled and optimised taking the dynamic range, which is a ratio of total force to uncontrollable force, to be objective function to be maximised. To achieve this goal, a general design guideline has been introduced for the Taguchi optimisation of the MR damper. In accordance with the presented guideline, nine candidate geometries have been identified to obtain optimal design, which is to be carried out by using Taguchi experimental design approach. In candidate damper geometries specified for solution of Taguchi approach, the gap width, flange (pole) thickness, radius of piston core and current excitation have been chosen as the variables with three different levels and piston gap length and piston diameter are constant values. The piston head housing thickness and coil width have been calculated to keep the magnetic flux density constant throughout the circuit, which ensures that one region of the magnetic circuit does not saturate prematurely and cause a bottleneck effect.

2 Design of MR damper

MR dampers operate on the following basic principle: a high-pressure fluid is forced through a small duct, resulting in a drop in pressure of the outgoing fluid. The pressure drop across a valve is caused by energy loss in the fluid due to plasticity and viscosity.

MR fluid flows through a gap in the piston head at aimed design of MR damper. Most devices that use controllable fluids can be classified as having either fixed poles (pressure-driven mode) or relatively moveable poles (direct-shear mode). Diagrams of these two basic operational modes are shown in Figure 1.

Figure 1 Basic operational modes for controllable fluid devices: (a) pressure-driven mode and (b) direct-shear mode

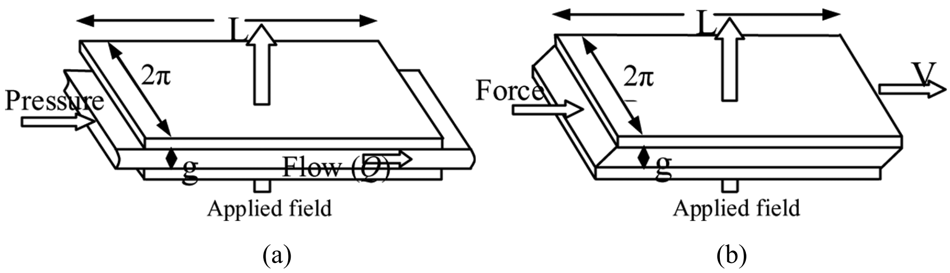

(a) (b)

Examples of valve mode devices include servo-valves and dampers. Examples of direct-shear mode devices include clutches, brakes, chucking and locking devices.

Figure 2 shows a schematic for the prototyped MR fluid damper under consideration. The chambers that are separated by the piston head are filled with MR fluid, whereas the accumulator, which is used for compensating the volume changes induced by the movement of the piston rod to the up and down, is filled with the pressurised nitrogen gas. During the motion of the MR damper's piston rod, fluid flows through the annular gap opened on the piston head. Inside the piston head, a coil is wound around the bobbin shaft with a heat-resistant and electrically insulated wire. When electrical current is applied to the coil, a magnetic field develops around the piston head.

Figure 2 Schematic for the prototyped MR shock damper

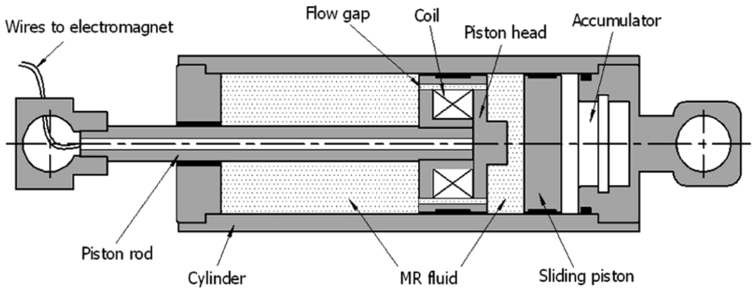

The magnetically induced iron particles inside the MR fluid line up in the direction of the magnetic flux lines to resist the flow producing a damping force. In the absence of a magnetic field, the MR fluid behaves like a Newtonian fluid. Therefore, the behaviour of MR fluid is often represented as Bingham plastic having a variable yield stress. The Bingham plastic model is given by

$$\tau = \tau_y(H)\operatorname{sgn}\left(\frac{\mathrm{d}u}{\mathrm{d}r}\right) + \mu\frac{\mathrm{d}u}{\mathrm{d}r} \quad |\tau| > |\tau_y| \tag{1}$$

$$\left(\frac{\mathrm{d}u}{\mathrm{d}r}\right) = 0 \quad |\tau| < |\tau_y| \tag{2}$$

where τ is the shear stress, τ_y is the dynamic yield stress, H is the applied magnetic field intensity, du/dr is the shear strain rate and μ is the plastic viscosity of the MR fluid.

Magnetic circuit under magnetic field applied to the MR damper with one-coil and annular gap, and some important dimensions are shown in Figure 3, the damper geometry is featured by gap length L, piston head housing thickness g_h, gap width g, flange (pole) thickness t, piston head radius R, radius of piston core R_c and coil width W.

Figure 3 MR damper configurations in a specified volume (see online version for colours)

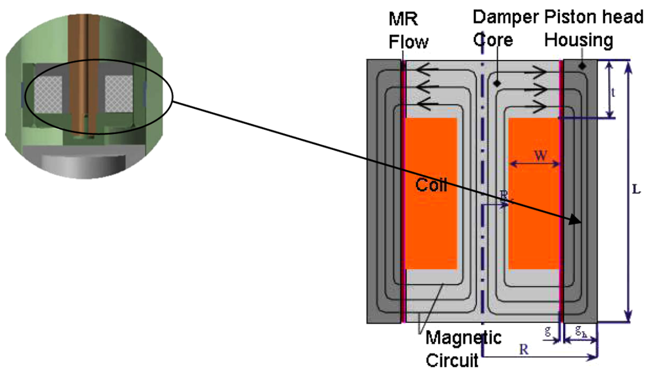

At the two ends of flanges, flux lines are perpendicular to the flow direction, which causes a field-dependent resistance on the flow. Pressure drop developed across the damper is calculated by

$$\Delta P = \Delta P_\mu + \Delta P_\tau = \frac{6Q\mu L}{\pi R_1 g^3} + 2\frac{tc}{g}\tau_y \tag{3}$$

where ΔP_μ and ΔP_τ are the viscous and uncontrollable pressure drop of MR damper. τ_y is yield stress, Q the flow rate through the MR shock damper, $Q = u_p(A_p - A_r)$, R_1 the average radius of the annular duct given by $R_1 = R - (g_h + 0.5g)$ and c is the coefficient that depends on the flow velocity profile and has a value ranging from a minimum value of 2.07 (for $\Delta P_\tau/\Delta P_\mu$ less than ~1) to a maximum value of 3.07 (for $\Delta P_\tau/\Delta P_\mu$ greater than ~100). Spencer et al. (1998) proposed the following approximate relation for the coefficient c

$$c = 2.07 + \frac{6Q\mu}{6Q\mu + 0.4\pi R_1 g^2 \tau_y}. \tag{4}$$

The minimum active volume, which is exposed to the magnetic field, is given by

$$V_e = k\left(\frac{\mu}{\tau_y^2}\right)\left(\frac{L}{2t}\right)\lambda W_m \tag{5}$$

where $k = 12/c^2$, $\lambda = \frac{\Delta P_\tau}{\Delta P_\mu}$ and $W_m = Q\Delta P_\tau$. By noting $V_e = 2\pi R_{1.2t} . g$, equation (5) can be further manipulated as follows:

$$\pi R_1 g^2\left(\frac{4t}{L}\right) = \frac{12}{c}\frac{\mu}{\tau_y}\lambda Q. \tag{6}$$

Equation (6) provides the geometric constraints and the aspect ratios needed for MR devices based on MR fluid properties, the desired control ratio and the device speed.

These equations assume that MR fluid specifications are known. Specifically, τ_y can be found in MR fluid specification sheets as a function of magnetic flux density.

MR fluid devices are usually designed such that the MR fluid can, or nearly, be magnetically saturated. It is under this condition that the fluid will generate its maximum yield stress τ_y. However, the yield stress τ_y that is used in the above-mentioned equations should be chosen from the MR fluid specification sheets to reflect the anticipated operating condition (Lord Corporation, 1999b).

2.1 Controllable force and the dynamic range

The total force generated by an MR shock damper consists of three components: Force due to the viscous effects F_μ, seal drag force (also friction force), which results from the relative motion between the mechanical components of the shock damper F_f, and field-dependent force F_τ, which is actually a result of induced iron particles inside the MR fluid. The sum of the first two is referred as uncontrollable force, since they generate a constant force according to any piston velocity, whereas the latter one is called the controllable force, as it varies with the applied field. A dimensionless parameter, dynamic range D, which is defined as the ratio of the total damper force to the uncontrollable force, is introduced to evaluate the overall performance of an MR damper:

$$D = 1 + \frac{F_\tau}{F_\mu + F_f} \tag{7}$$

where

$$F_\mu = u_p (A_p - A_r) \frac{6\mu L A_p}{\pi R_1 g^3} \tag{8}$$

$$F_\tau = 2c \frac{t}{g} A_p \tau_y \operatorname{sgn}(u_p) \tag{9}$$

which reveals that controllable force is inversely proportional to the gap size g. The dynamic ratio D is desired to be as large as possible to maximise the effectiveness of an MR damper. As shown in equations (8) and (9), the viscous force increases two orders of magnitude faster than the controllable force with a small gap size if one assumes that the magnetic field is saturated; consequently, the dynamic range tends to zero. As the gap size becomes large, both the controllable force and the viscous force decrease. Note that the friction force is a constant, so again the dynamic range tends to zero. It is obvious that an optimal dynamic range must exist (Delivorias, 2004).

The dynamic range, equation (7), can be rewritten as:

$$D = 1 + \frac{2ctA_p\tau_y}{(A_p - A_r)\dfrac{6\mu L u_p A_p}{\pi R_1 g^2} + gF_f}. \tag{10}$$

Delivorias (2004) specified that the dynamic range has to be greater than 2.6. This means that the controllable force must be a factor 2.6 greater than the viscous forces. Too small gap values will lead to a dynamic range, which will be nearly zero. To obtain a sufficient amount of controllable force, the gap has to be quite narrow. In addition, parameters such as the piston radius, the yield stress and the gap width will play an important role in searching for the right design.

The more important stage in the design considerations of an MR damper is the magnetic circuit design provided changes in the viscosity of the MR fluid.

3 Calculating magnetic flux density

As can be seen in Figure 3, the MR damper is shaped to guide the magnetic flux axially through the bobbin, across the bobbin flange (pole) thickness and gap at the one end, through the flux return, and across the gap and bobbin flange (pole) thickness again at the opposite end. The fluid volume through which the magnetic field passes is defined as the active volume. MR effects only occur within this active volume. For most effective dampers, it is needed to have a high magnetic flux density passing through a large active volume. However, large numbers of magnetic coils are required for producing large magnetic fields. For an MR fluid device with constant radius and height, more volume devoted to magnetic coils translate directly to a smaller active volume. Moreover, more volume devoted to the coils left less volume for the magnetically permeable carrier materials (Bölter and Janocha, 1997). An optimised circuit would maintain a balance between the field produced and power required by the magnetic coils, and a valve design that would make best use of the field to activate the MR fluid yield stress (Rosenfeld and Wereley, 2004).

In this study, the hydrocarbon-based MR fluid product (MRF-132DG) from Lord Corporation was used. By applying the least-squares curve fitting method to the fluid property specifications (Lord Corporation, 2003), the yield stress was determined to be

$$\tau_y = 52.962B^4 - 176.51B^3 + 158.79B^2 + 13.708B + 0.1442. \tag{11}$$

In equation (11), the unit of the yield stress τ_y is kPa while that of the magnetic flux density is Tesla (T).

To calculate the pressure drop across the MR dampers, it is necessary to solve the magnetic circuit equations. After the magnetic circuit solution, the yield stress of MR fluid in the active volume can be obtained from equation (11) and then the pressure drops can be calculated using equation (3) (Nguyen et al., 2008).

Magnetic flux density changes with the applied current excitation. Then, an expression must be defined between magnetic flux density and current. The magnetic circuit can be analysed using the magnetic Kirchoff's law as follows:

$$\sum H_s l_s = N_c L \tag{12}$$

where H_s is the magnetic field intensity in the sth link of the circuit and l_s is the overall effective length of sth link. N_c is the number of turns of the coils and I is the applied current excitation in the coil. The magnetic flux conservation rule of the circuit is given by

$$\Phi = B_s A_s \tag{13}$$

where Φ is the magnetic flux of the circuit, A_s and B_s are the cross-sectional area and magnetic flux density of the sth link, respectively. Relationship between the magnetic flux density and magnetic field intensity is given as $B_s = \mu_0 \mu_r H_s$, where μ_0 is the magnetic permeability of free space ($\mu_0 = 4\pi \times 10^{-7}$ TmA^{-1}) and μ_r is the relative permeability and this is a material constant. Relative permeability has significant impact on the calculation of magnetic flux density, and especially relative permeability of MR fluid. This relationship is valid at relatively low magnetic fields. As the magnetic field becomes larger, then its ability to polarise the magnetic material diminishes and the material is almost magnetically saturated (Nguyen et al., 2008). B–H curve is used to express the magnetic property of material.

For the single-coil annular MR damper that would be desired for optimal design, magnetic circuit can be seen in Figure 4.

Equations (12) and (13) can be rewritten as

$$2H_1l_1 + 2H_2l_2 + 2H_3l_3 + H_4l_4 + H_8l_8 = N_cI \tag{14}$$

$$\Phi = B_1A_1 = B_2A_2 = B_3A_3 = B_4A_4 = B_8A_8. \tag{15}$$

The effective length and cross-sectional area of the magnetic links are given as follows:

$$l_1 = l_7 = R_1 - 0.5(R_c + g); \quad l_2 = l_6 = g;$$

$$l_3 = l_5 = 0.5 g_h; \quad l_4 = l_8 = L - t$$

$$A_1 = A_7 = 2\pi R_c t; \quad A_2 = A_6 = 2\pi R_1 t;$$

$$A_3 = A_5 = 2\pi\left(R - \frac{3g_h}{4}\right)t; \quad A_4 = \pi\left(R^2 - \left(R - \frac{g_h}{2}\right)^2\right); \quad A_8 = \pi R_C^2.$$

At the lower magnetic fields, the magnetic flux density in the gap can be expressed by equations (14) and (15) as follows (Nguyen and Choi, 2009b):

$$B_2 = \frac{\mu_0 N_c I}{2\frac{g}{\mu_{r,m}} + 2\frac{A_2 l_1}{\mu_{r,c} A_1} + 2\frac{A_2 l_3}{\mu_{r,c} A_3} + \frac{A_2 l_4}{\mu_{r,c} A_4} + \frac{A_2 l_8}{\mu_{r,c} A_8}} \tag{16}$$

where $\mu_{r,m}$ and $\mu_{r,c}$ are the relative permeability of MR fluid and piston, respectively. N_c is the number of coil turns, which can be approximated by $N_c = A_c/A_w$, and A_c is the cross-sectional area of the coil and A_w is the cross-sectional area of the wire.

Figure 4 Simplified magnetic circuit of MR shock damper (see online version for colours)

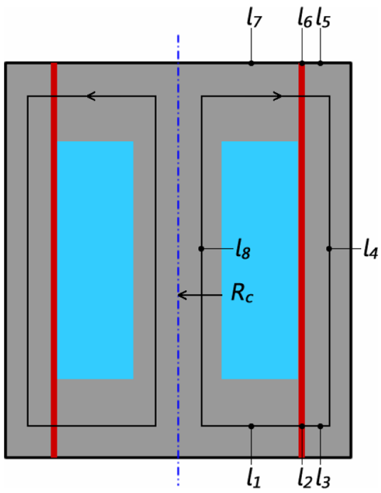

It is very difficult to measure exact relative permeability of materials (Karakoc et al., 2008). Relative permeability is a function of temperature and applied magnetic field intensity. It decreases as the temperature increases and also materials lose their magnetic properties after a finite temperature is reached, which is the so-called Curie Point. Whenever a material is heated up to its Curie temperature, its permeability will converge to 1, thus it will behave as a paramagnetic material. Therefore, low carbon steel having a high magnetic permeability and saturation is desired. Ideally, the carbon content of the steel should be less than 0.15% (Lord Corporation, 1999a).

In the study, low carbon steel C1010 steel was used as the piston material. B–H curves of C1010 steel (Salvetti, 2004) and MRF-132DG MR fluid (Lord Corporation, 2008) can be seen in Figures 5 and 6, respectively.

Figure 5 B–H curve of C1010 steel (see online version for colours)

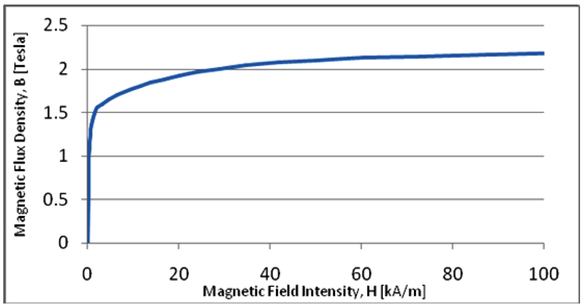

Figure 6 B–H curve of MRF-132DG (see online version for colours)

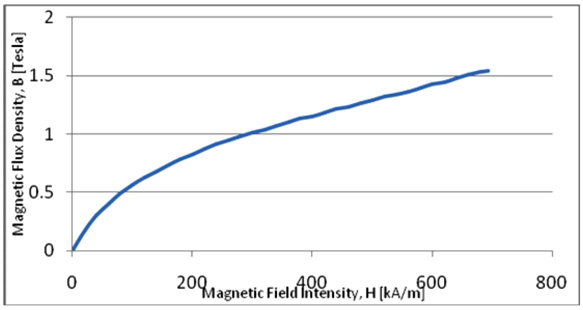

A feasible candidate geometry can be considered alone in which the various critical areas through which the magnetic field passes are the same size. This is necessary to keep the magnetic flux density constant throughout the circuit, which ensures that one region of the magnetic circuit does not saturate prematurely and cause a bottleneck effect (Rosenfeld and Wereley, 2004). There are three critical areas in the magnetic circuit: the circular cross-section of the bobbin core A_{Rc}, the annular cross-sectional area of the flux return A_{gh}, and the cylindrical area at the interior of the bobbin flanges A_{tc}. These critical areas are expressed as follows:

$$A_{Rc} = \pi R_c^2 \tag{17}$$

$$A_{gh} = \pi[R^2 - (R_c + W + g)^2] \tag{18}$$

$$A_{tc} = 2\pi R_c t. \tag{19}$$

In the analytical optimisation method proposed by Rosenfeld and Wereley (2004), the coil width (W), the flange (pole) thickness (t) and piston head housing thickness (g_h) were calculated. Equating equations (17) and (18), and rearranging into the quadratic form for positive W yielded

$$W = -(g + R_c) + \sqrt{R^2 - R_c^2}. \tag{20}$$

Setting equation (17) equal to equation (19), t is

$$t = \frac{1}{2} R_c \tag{21}$$

$$g_h = R - (W + g + R_c). \tag{22}$$

Nguyen et al. (2007) showed that this assumption is true for the coil width and the piston head housing thickness but not for the flange thickness because the damping ratio ($\lambda = \Delta P_\tau / \Delta P_\mu$) depends not only on the magnetic flux density through the MR duct but also on the flange thickness. To this respect, in this study, equations (20) and (22) were used to determine optimal geometry. The flange (pole) thickness was taken as the design variable.

4 Taguchi experimental design method for optimal MR damper configuration

Design of Experiments (DOE) is a statistical technique used to study the effects of multiple variables simultaneously. Dr. Genechi Taguchi was a Japanese scientist who researched ways to improve the quality of manufactured products. The quality engineering method that Taguchi proposed is commonly known as the Taguchi method. For laying out experiments, he created a number of special orthogonal arrays, each of which is used for a number of experimental situations. His use of the Signal-to-Noise (S/N) ratio for analysis of repeated results helps experimenters easily assure a design that is robust to the influence of uncontrollable factors (Roy, 2003). Use of orthogonal arrays to design experiments is the key. Full factorial experiments are too numerous to do. Orthogonal arrays were developed to make the DOE technique more applicable by reducing the size of the experiments (Roy, 2003). Taguchi strongly recommends use of S/N ratio to capture the variability of data within the group and thus to measure quality characteristic and then determine optimum conditions.

Taguchi proposed that three S/N ratio equations depending on the desirability of results quality characteristic can be of type bigger is better, smaller is better, or nominal is best (Table 1).

Table 1 Signal-to-Noise (S/N) ratio equations

Quality characteristic	*S/N ratio*
Smaller is better	$-10\log\left(\frac{1}{n}\sum y_i^2\right)$
Nominal is best	$-10\log\left(\frac{1}{n}\sum (y_i - y_0)^2\right)$
Bigger is better	$-10\log\left(\frac{1}{n}\sum \frac{1}{y_i^2}\right)$

While increasing S/N ratio, variation around the target value decreases, then higher S/N values is desirable. Regardless of original results, S/N ratio is always wanted as bigger is better.

4.1 Geometrical optimisation of MR damper using Taguchi experimental design method

The objective of the study is to obtain optimum dimensions of four parameters (gap, flange thickness, radius of piston core, current excitation), which are expected to maximise the dynamic range of the MR damper. Three different levels have been specified for each of the parameters under consideration (Table 2).

Convenient orthogonal array depending on the number of factors and levels was selected. For the selected three levels, the Degree of Freedom (DOF) is 3 – 1 = 2, and for four factors, total DOF is 4 × 2 = 8, since L9 array was specified (Table 3). Nine damper models have been analysed in accordance with Taguchi's L9 array (Table 4). Dynamic range was specified as the response value.

Table 2 Parameters and levels, which were used for Taguchi method

Parameter	*Level 1*	*Level 2*	*Level 3*
Gap (g)	0.4 mm	0.8 mm	1.2 mm
Flange thickness (t)	2 mm	3 mm	4 mm
Core (R_c)	5 mm	6 mm	7 mm
Current (I)	0.2 A	0.4 A	0.6 A

Table 3 L9 orthogonal array

Exp. No.	*Factor 1*	*Factor 2*	*Factor 3*	*Factor 4*
1	1	1	1	1
2	1	2	2	2
3	1	3	3	3
4	2	1	2	3
5	2	2	3	1
6	2	3	1	2
7	3	1	3	2
8	3	2	1	3
9	3	3	2	1

Table 4 Factors assigned to L9 orthogonal array

Exp. No.	*Gap* (g) *(mm)*	*Flange* (t) *(mm)*	*Core* (R_C) *(mm)*	*Current* (I) *(A)*
1	0.4	2	5	0.2
2	0.4	3	6	0.4
3	0.4	4	7	0.6
4	0.8	2	6	0.6
5	0.8	3	7	0.2
6	0.8	4	5	0.4
7	1.2	2	7	0.4
8	1.2	3	5	0.6
9	1.2	4	6	0.2

As can be seen from Table 5, the coil width and the piston head housing thickness were calculated using equations (20) and (22), respectively. Number of turns of the coil was calculated considering that coil wire diameter is 0.516 mm (24-gauge) and 1 mm and 2 mm insulation material on the inner and outer faces of coil width, respectively.

Table 5 Dimensions of coil width, piston head housing thickness and number of turns of the coil

Exp. No.	*Coil width* (W) (*mm*)	*Piston head housing* (g_h) (*mm*)	*Number of turns of the coil* (N_c)
1	12.20	1.00	548
2	10.84	1.37	433
3	9.40	1.80	320
4	10.44	1.37	408
5	9.00	1.80	296
6	11.80	1.00	522
7	8.60	1.80	273
8	11.40	1.00	495
9	10.04	1.37	382

To calculate yield stress of MRF132DG depending on magnetic flux density given equation (11), the magnetic flux density has to be calculated. For this purpose, the values of the relative permeability can be determined from B–H curves in Figures 5 and 6 by knowing that $\mu_r = B_K/\mu_0 H_k$ for which $\mu_0 = 4\pi \times 10^{-7}$ TmA^{-1}. Relative permeabilities were calculated for C1010 steel and MRF132DG as $\mu_{r,c} \cong 1240$ and $\mu_{r,m} \cong 3$, 3.5 and 4, respectively. Relative permeability of MR fluid is a very important parameter to calculate magnetic flux density. A minimal changing of that causes an important changing on magnetic flux density. MR fluid devices are usually designed such that the MR fluid can be magnetically saturated. The saturation values are not known exactly at which the values of magnetic flux density occurred. Because of that, $\mu_{r,m}$ was specified as three different values. Thus, experiment results were obtained for each $\mu_{r,m}$. It was assumed that core material and piston rod material have same relative permeability. Magnetic flux densities and yield stresses were calculated as follows (Table 6):

Table 6 Magnetic flux density and yield stress

Exp. No.	*Magnetic flux density* (B) (*Tesla*)			*Yield stress* (τ_y) (*kPa*)		
	R_1	R_2	R_3	R_1	R_2	R_3
1	0.52	0.60	0.69	29.03	34.42	39.15
2	0.82	0.95	1.09	44.64	48.32	49.91
3	0.90	1.06	1.21	47.29	49.69	50.05
4	0.58	0.67	0.77	32.87	38.35	42.84
5	0.14	0.16	0.19	4.69	5.86	7.11
6	0.49	0.57	0.66	27.41	32.70	37.45
7	0.17	0.20	0.23	6.32	7.92	9.62
8	0.47	0.54	0.62	25.69	30.83	35.56
9	0.12	0.14	0.16	3.78	4.71	5.71

Pressure drop through gap can be calculated by equation (3) for each experiment. In these calculations, we have taken the piston head diameter to be 40 mm, piston rod diameter to be 10 mm and piston velocity to be 0.2 m/s. Controllable pressure drop, uncontrollable pressure drop and control ratio are given in Table 7. Uncontrollable force, controllable force and dynamic range were calculated by equations (8)–(10), respectively (Table 8). Friction force was assumed to be a constant force of 30 N.

Table 7 Pressure drop and control ratio

Exp. No.	c			ΔP_μ (kPa)			ΔP_τ (kPa)			λ		
	R_1	R_2	R_3	R_1	R_2	R_3	R_1	R_2	R_3	R_1	R_2	R_3
1	2.61	2.57	2.54	619.3	619.3	619.3	758.4	884.6	993.6	1.2	1.4	1.6
2	2.51	2.49	2.48	631.7	631.7	631.7	1680.9	1805.3	1858.8	2.7	2.9	2.9
3	2.50	2.49	2.49	646.7	646.7	646.7	2366.2	2474.4	2490.5	3.7	3.8	3.9
4	2.28	2.26	2.24	79.8	79.8	79.8	375.1	432.9	480.2	4.7	5.4	6.0
5	2.73	2.68	2.63	81.7	81.7	81.7	95.9	117.6	140.4	1.2	1.4	1.7
6	2.31	2.28	2.26	78.3	78.3	78.3	633.3	745.5	845.7	8.1	9.5	10.8
7	2.46	2.41	2.37	24.5	24.5	24.5	51.9	63.6	75.9	2.1	2.6	3.1
8	2.20	2.18	2.17	23.4	23.4	23.4	282.8	336.5	385.6	12.1	14.4	16.5
9	2.58	2.53	2.48	23.9	23.9	23.9	65.1	79.4	94.5	2.7	3.3	4.0

Table 8 Controllable force, uncontrollable force and dynamic range

Exp. No.	F_μ (N)			F_τ (N)			D		
	R_1	R_2	R_3	R_1	R_2	R_3	R_1	R_2	R_3
1	778.30	778.30	778.30	953.06	1111.66	1248.62	2.18	2.38	2.54
2	793.78	793.78	793.78	2112.33	2268.55	2335.81	3.56	3.75	3.84
3	812.69	812.69	812.69	2973.51	3109.36	3129.65	4.53	4.69	4.71
4	100.31	100.31	100.31	471.40	544.01	603.39	4.62	5.17	5.63
5	102.73	102.73	102.73	120.57	147.82	176.39	1.91	2.11	2.33
6	98.33	98.33	98.33	795.84	936.81	1062.75	7.20	8.30	9.28
7	30.78	30.78	30.78	65.21	79.93	95.41	2.07	2.31	2.57
8	29.45	29.45	29.45	355.38	422.80	484.58	6.98	8.11	9.15
9	30.05	30.05	30.05	81.85	99.80	118.78	2.36	2.66	2.98

4.2 Parameter optimisation

The impact of the specified factors and levels on results can be examined using Taguchi experimental design method and thus it was allowed that optimal geometry could be obtained. Dynamic range was specified as response value. Bigger dynamic range is best for MR damper, this means of controllable force much bigger than uncontrollable force. Therefore, the ‘Bigger is Best’ was specified as S/N ratio equation. Dynamic ranges and calculated S/N ratios can be seen in Table 9.

In addition, S/N ratios of the each level of the factors are calculated in Table 10 and the ratios can be seen in Figure 7. After the S/N ratio analysis, best levels for each factor are specified in Table 11.

Figure 7 S/N ratios

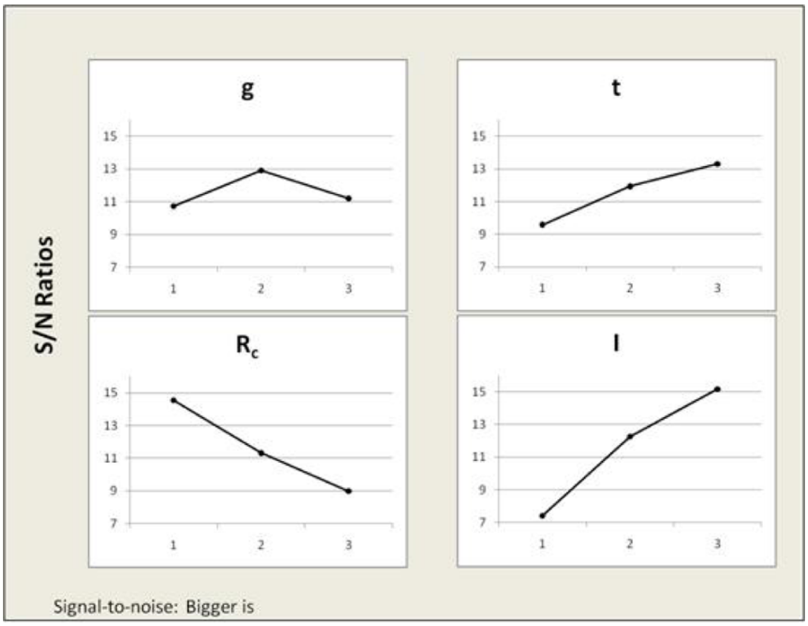

Table 9 Dynamic ranges and S/N Ratios for L9 array

Exp. No.	*g*	*t*	R_c	*I*	R_1	R_2	R_3	*S/N*
1	1	1	1	1	2.18	2.38	2.54	7.432
2	1	2	2	2	3.56	3.75	3.84	11.390
3	1	3	3	3	4.53	4.69	4.71	13.333
4	2	1	2	3	4.62	5.17	5.63	14.134
5	2	2	3	1	1.91	2.11	2.33	6.427
6	2	3	1	2	7.20	8.30	9.28	18.199
7	3	1	3	2	2.07	2.31	2.57	7.196
8	3	2	1	3	6.98	8.11	9.15	17.988
9	3	3	2	1	2.36	2.66	2.98	8.401

Table 10 S/N ratios for each level of factors

Level	*g*	*t*	R_c	*I*
1	10.72	9.59	14.54	7.42
2	12.92	11.94	11.31	12.26
3	11.20	13.31	8.99	15.15

Table 11 Specified optimum levels of S/N ratio

Parameters	*Optimum level*	*Value*
g	2	0.8 mm
t	3	4 mm
R_c	1	5 mm
I	3	0.6 A

The dynamic range and S/N ratio for these optimal parameter values are found to be 11.33 and 21.086, respectively (Table 12). These values are best among others given in Table 9. Therefore, the values show an optimal selection after S/N analysis. The optimal dimensions of MR damper using Taguchi experimental design method are summarised in Table 13.

Table 12 S/N ratio and dynamic range at optimum levels

Levels	*S/N*	*Dynamic range*
Gap: 2 Flange thickness: 3 Core: 1 Current: 3	21.086	11.33

Table 13 Optimum geometry

g	0.8 mm
t	4 mm
R_c	5 mm
I	0.6 A
W	11.8 mm
g_h	1 mm

Interaction among factors is quite common. A good understanding of interaction between two factors is highly effective in interpreting the experimental results. Therefore, it is important how to design experiments to include interactions and how to analyse results to determine that if interaction is present whether it is significant, or which factor levels are most desirable. An interaction between factors is something that changes the way the factors involved influence the results. An interaction is neither a factor, as cannot be controlled it, nor a result, since it has an effect on the result (Roy, 2003). Interactions among factors for our study can be seen in Table 14.

The numbers under the SI column show the calculated value of the Severity Index (SI). The optimum levels column lists the desirable levels for the interacting factors. The numbers [3, 1] for Flange thickness × Core in the first row indicate that level 3 of Flange thickness and level 1 of Core are the desirable levels. These levels for the factors should be adjusted to compensate for interaction effects.

Table 14 Interactions among the various factors

Interacting factor pairs	*SI* (%)	*Optimum levels*
Flange thickness × Core	56.49	3 and 1
Gap × Flange thickness	49.54	2 and 3
Gap × Core	34.08	2 and 1
Gap × Current	33.18	2 and 3
Core × Current	32.94	1 and 3
Flange thickness × Current	22.07	3 and 3

4.3 ANOVA

The effect of each individual parameter on the final results can be determined by using Analysis of Variance (ANOVA). ANOVA is a statistical tool and a mathematical technique that separates the components of the total variation. The main objective of ANOVA is to extract from the results how much variation each factor causes relative to the total variation observed in the result (Roy, 2003).

The results of the ANOVA are shown in Table 15. The effect of each factor on the performance of MR damper is clearly seen in this table. It is clear from Table 15 that the most significant parameter is the current excitation contributing percentage 54.64 followed by core radius percentage 27.85.

Table 15 ANOVA computation

	DOF	*Sum of squares* (S)	*Variance* (V)	*Percent* (P %)
Gap	2	8.05	4.025	4.80
Flange thickness	2	21.27	10.63	12.69
Core	2	46.68	23.34	27.85
Current	2	91.56	45.78	54.64
Error	0			

The error term will always be zero when the error DOF is zero as seen in Table 15. It not necessarily means that there is no experimental error or that there are no effects from the factors not included in the experiment. It simply means that there was no provision in the experiment to capture the experimental error. The error term is meaningful only when the error DOF is non-zero. When any factor is pooled, error term is generated.

The gap in which the MR fluid passes has the smallest *S* (8.051) and it is also less than 10% of the highest *S* (91.563). Thus, this factor should be pooled (Roy, 2003). Theoretically, the factor pooled offers opportunities to treat them like uncontrollable factor. When gap factor is pooled, ANOVA terms can be recalculated. Theoretically, the factor pooled offers opportunities to treat them like uncontrollable factor.

In Table 16 can be seen ANOVA computation after pooling factor *g*.

Table 16 ANOVA computation after pooling factor *g*

	Degree of Freedom (*DOF*)	*Sum of Squares* (S)	*Variance* (V)	*F-ratio*	*Percent* (*P %*)
Gap	–	–	–	–	–
Flange th.	2	21.274	10.637	2.642	7.89
Core	2	46.686	23.343	5.798	23.054
Current	2	91.563	45.781	11.372	49.835
Error	2	8.051	4.025		19.221

Error term represents not just any experimental or analytical error. It also represents the collective influence of all factors not included in the study, plus any experimental error if present. Regardless of the magnitude of the influence of the error term, the relative influence of the individual significant factors is useful information (Roy, 2003).

Confidence Interval (CI) represents the boundaries on the expected results and is always calculated at a confidence level. The CI is calculated using ANOVA values. CI specifies the boundaries of the expected performance at the optimum condition.

Confidence interval is calculated as follows:

$$\mathrm{CI} = \pm\left[\frac{F(1, n_2) \times V_e}{N_e}\right]^{0.5} \tag{23}$$

where $F(1, n_2)$ is the F value from the F table for factor DOF and error DOF at the confidence level desired, V_e the variance of the error term (from ANOVA) and N_e is the effective number of replications.

When gap is pooled, CI can be calculated as follows,

$$\mathrm{CI} = \pm\left[\frac{3.5 \times 4.02577}{1.29}\right]^{0.5} = \pm 3.31 \quad \text{for confidence level 90\%.}$$

Since the CI was calculated at a 90% confidence level, if several such sets are tested, 9 out of 10 times the averages of the sets are expected to fall within these limits. According to values in Table 10, predicted S/N for overall optimum condition is calculated as follows

$$\frac{S}{N_{\text{predicted}}} = \frac{S}{N_{g,2}} + \frac{S}{N_{t,3}} + \frac{S}{N_{Rc,1}} + \frac{S}{N_{c,3}} - 3\overline{T}$$

$$\frac{S}{N_{\text{predicted}}} = 12.92 + 13.31 + 14.54 + 15.15 - 3\frac{104.5}{9} = 21.086.$$

Therefore, for 90% confidence level, CI is found as

$$(21.086 - 3.31) < \mathrm{CI} < (21.086 + 3.31)$$

$$17.776 < \mathrm{CI} < 24.396.$$

A confirmation analysis is conducted to check whether the obtained optimum condition really produces the desired responses

$$\frac{S}{N} = -10 \log\left[\frac{1}{3}\left(\frac{1}{10.11^2} + \frac{1}{11.06^2} + \frac{1}{11.11^2}\right)\right] = 20.616$$

The value is contained within the CI at 90%, which means that the optimum condition is confirmed by test of significance. Specified optimal geometry is confirmed with the result.

5 Conclusions

In this study, an MR damper optimisation model was proposed. Taguchi experimental design approach was used for the optimisation model. Taguchi method has been shown to present an effective optimisation. The gap, flange thickness, radius of piston core and current excitation factors were determined to achieve candidate geometries. While determining the factors it was needed to consider ease of manufacturing. Three levels are specified for each of the factors. The results of MR damper were obtained analytically. Dynamic range was a key parameter to be evaluated by Taguchi approach, so dynamic range was response value and it was desired to obtain the highest value of the dynamic range. Nine damper geometries were analysed in accordance with Taguchi's L9 array for 4 factors and 3 levels of each of them. As a result of the Signal-Noise analysis and ANOVA, optimal geometry represented that the highest value of the dynamic range was obtained.

After Taguchi experimental design analysis, it can be seen that gap is minimum effect on damper performance. One of the most important reasons of the result is that chosen gap levels are close to providing maximum dynamic range. According to CI at 90%, gap and flange thickness factors have lower confidential levels than the value. So, the two factors can be considered insignificant and are raised error term. The factors should be specified based on ease of manufacturing than that prescribed by the optimum condition for the study. In addition, the influences of factors are relative; they can be different from another study according to specified factors.

Acknowledgement

The authors gratefully acknowledge TUBITAK for making this project possible under Grant Nos. 104M157 and 108M635.

References

Bölter, R. and Janocha, H. (1997) 'Design rules of MR fluid actuators in different working modes', *Proc. SPIE*, Vol. 3045, pp.148–159.

Delivorias, R.P. (2004) *Application of ER and MR fluid in an Automotive Crash Energy Absorber*, Eindhoven University of Technology Department of Mechanical Engineering, Eindhoven, Report No. MT04.18.

Hitchcock, G.H. (2002) *A Novel Magneto-Rhelogical Fluid Damper*, Master Thesis, Mechanical Engineering Department of University of Nevada, Reno.

Jolly, M.R., Bender, J.W. and Carlson, J.D. (1999) 'Properties and applications of commercial magnetorheological fluids', *Journal of Intelligent Material Systems and Structures*, Vol. 10, pp.5–13.

Karakoc, K., Park, E.J. and Suleman, A. (2008) 'Design considerations for an automotive magnetorheological brake', *Mechatronics*, Vol. 18, pp.434–447.

Lord Corporation (1999a) *Magnetic Circuit Design*, Engineering Note, http://www.lord.com/Portals/0/MR/Magnetic_Circuit_Design.pdf

Lord Corporation (1999b) *Designing with MR Fluids*, Engineering Note, http://www.lord.com/Portals/0/MR/designing_with_MR_fluids.pdf

Lord Corporation (2003) *MR Fluid Product Bulletins*, http://www.rheonetic.com/fluid begin.htm

Lord Corporation (2008) *MRF-132DG Magneto-Rheological Fluid*, Lord Technical Data, http://www.lordfulfillment.com/upload/DS7015.pdf

Namuduri, C.S., Alexandridis, A.A., Madak, J. and Rule, D.S. (2001) *Magnetorheological Fluid Damper with Multiple Annular Flow Gaps*, 6,279,701 US Patent Specification.

Nguyen, Q.H., Han, Y.M., Choi, S.B. and Wereley, N.M. (2007) 'Geometry optimization of MR valves constrained in a specific volume using the finite element method', *Smart Materials and Structures*, Vol. 16, pp.2242–2252.

Nguyen, Q.N., Choi, S.B. and Wereley, N.M. (2008) 'Optimal design of magnetorheological valves via a finite element method considering control energy and a time constant', *Smart Materials and Structures*, Vol. 17, p.12.

Nguyen, Q.H. and Choi, S.B. (2009a) 'Dynamic modeling of an electrorheological damper considering the unsteady behavior of electrorheological fluid flow', *Smart Materials and Structures*, Vol. 18, p.8.

Nguyen Q.N. and Choi, S.B. (2009b) 'Optimal design of MR shock absorber and application to vehicle suspension', *Smart Materials and Structures*, Vol. 18, p.11.

Rosenfeld, N.C. and Wereley, N.M. (2004) 'Volume-constrained optimization of magnetorheological and electrorheological valves and dampers', *Smart Material and Structure*, Vol. 13, pp.1303–1313.

Roy, R.K. (2003) *Design Experiments using the Taguchi Approach: 16 Steps to Product and Process Improvement*, A Wiley-Interscience Publication, New York.

Salvetti, M. (2004) *Detector Solenoid: Thermal and Structural Analyses*, Magnet Documents, http://meco.ps.uci.edu/old/magnet_docs/mm056.pdf

Spencer, B.F., Yang, G., Carlson, J.D. and Sain, M.K. (1998) "Smart' dampers for seismic protection of structures: a full-scale study', *Second World Conference on Structural Control*, 28 June–1 July, Kyoto, Japan.

Stanway, R., Sproston, J.L. and El-Wahed, A.K. (1996) 'Applications of electro-rheological fluids in vibration control: a survey', *Smart Material and Structures*, Vol. 5, pp.464–482.

Wereley, N.M. and Pang, L. (1998) 'Nondimensional analysis of semi-active electrorheological and magnetorheological dampers using approximate parallel plate models', *Smart Material and Structures*, Vol. 7, pp.732–743.

Yang, L., Fubin, D.F. and Eriksson, A. (2008) 'Analysis of the optimal design strategy of a magnetorheological smart structure', *Smart Materiral and Structures*, Vol. 17, p.8.

Zhang, H.H., Liao, C.R., Chen, W.M. and Huang, S.L. (2006) 'A magnetic design method of MR fluid dampers and FEM analysis on magnetic saturation', *Journal of Intelligent Material Systems And Structures*, Vol. 17, pp.813–818.

Nomenclature

τ	Shear stress
τ_y	Dynamic yield stress
H	Magnetic field intensity
du/dr	Shear strain rate
(	Plastic viscosity
ΔP	Total pressure drop
ΔP_μ	Viscous pressure drop
ΔP_r	Yield pressure drop
Q	Volume flow rate
L	Length of the flow channel
g	Gap width
R_1	Average radius of the annular duct
t	Flange (pole) thickness
c	Coefficient depending on flow velocity
R	Piston head radius
R_C	Radius of piston core
W	Coil width
u_p	Piston velocity
A_p	Piston head cross-sectional area
A_r	Piston rod cross-sectional area
g_h	Piston head housing thickness
T	Dimensionless yield stress
V_e	Minimum active volume
λ	Control ratio
W_m	Mechanical power level
D	Dynamic range
F_μ	Viscous force
F_τ	Yield force
F_f	Friction force
F	Total damping force
B	Magnetic flux density
l_s	Overall effective length of sth link of magnetic circuit
N_C	Number of turns of the coils
I	Applied current excitation
Φ	Magnetic flux of the circuit
A_S	Cross sectional area of the sth link of magnetic circuit
μ_0	Magnetic permeability of free space
μ_r	Relative permeability

$\mu_{r,m}$	Relative permeability of MR fluid
$\mu_{r,c}$	Relative permeability of piston material
A_c	Cross-sectional area of the coil
A_w	Cross-sectional area of the wire
A_{Rc}	Circular cross-section of the bobbin core
A_{gh}	Annular cross-sectional area of the flux return
A_{tc}	Cylindrical area at the interior of the bobbin flanges
R_k	Channel radius for cable in piston rod
S/N	Signal-to-noise ratio
y_0	Target value
DOF	Degree of Freedom
S	Sum of squares
V	Variance
CI	Confidence interval
$F(1, n_2)$	F value from the F table
V_e	Variance of the error term
N_e	Effective number of replications

All units are SI base units.